Modeling of Various Kinds of Applicators Used for Microwave Hyperthermia Based on the FDTD Method

Jean-Christophe Camart, David Despretz, Maurice Chivé, and Joseph Pribetich

Abstract— **This paper presents the modeling using the finite difference time domain (FDTD) method of interstitial and endocavitary applicators which have been designed and developed for microwave hyperthermia treatments controlled by microwave radiometry. For each kind of applicators, the numerical results are given concerning the reflection coefficient S_{11}, the power deposition, and the heating patterns. These results are compared with the measurements performed on phantom models of human tissues and show a good agreement. Possibilities of future developments are discussed.**

I. Introduction

A LARGE number of devices have been designed in order to produce therapeutic heating by microwave hyperthermia of tumors having different sizes and located in various places of the human body. Among these devices, we have been interested for more than a decade, in the study of various kinds of applicators.

1) Coaxial antenna for interstitial hyperthermia generally used for deep-seated tumors.
2) Endocavitary applicators used for thermotherapy of the prostate.

The particularity of these applicators lies in their double role: on one hand, to transfer the energy delivered by the microwave generator to the tissues to be heated and, on the other hand, to pick up the thermal noise in order to determine the radiometric temperature.

In all cases the main problem to characterize these applicators is the determination of the radiating pattern at the heating frequency (power deposition) but also the determination of the pattern which contributes to the noise power when these applicators operate for radiometry (generally around 3 GHz) [1]. The research works undertaken in this domain aim at increasing the efficiency of the heating of tumors in volume and in depth. In this paper, the results (theoretical study and experimental verifications) concerning these applicators, are presented.

In Section II, the different structures which have been studied are described. In Section III, the modeling of the applicators which is based on the finite difference time domain (FDTD) method is briefly described. The theoretical determination of the heating pattern is also reviewed in this section. Section IV is concerned with experimental measurements in order to characterize these applicators. In Section V, which is the major part of this paper, the main results obtained with these devices are given. Finally, Section VI is devoted to concluding remarks and further considerations on this work.

Manuscript received November 10, 1995; revised May 3, 1996.

The authors are with the IEMN-UMR CNRS No. 9929, Département Hyperfréquences et Semiconducteurs (CHS), Domaine Scientifique et Universitaire de Villeneuve D'Ascq, 59652 Villeneuve D'Ascq Cedex, France.

Publisher Item Identifier S 0018-9480(96)07027-5.

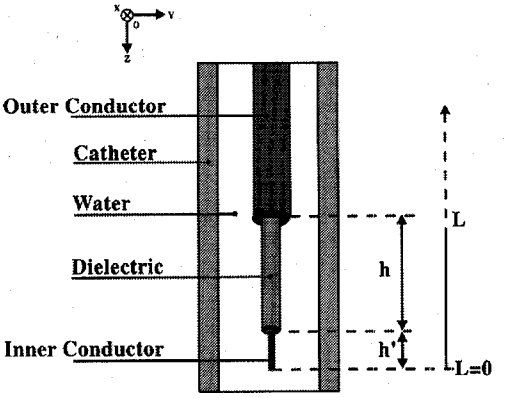

Fig. 1. Description of the interstitial applicator made from a coaxial cable inserted in an implanted plastic catheter.

II. Description of the Applicators

A. Interstitial Applicators

The interstitial applicator is made from a UT34 standard coaxial cable 0.034″ (0.85 mm) in external diameter, of 50 Ω characteristic impedance. At the end of this coaxial cable the external conductor was removed over a length h and the central core totally stripped on a length h' (Fig. 1). This miniature antenna is inserted into the same standard plastic catheter used for brachytherapy. This catheter is filled with water.

B. Endocavitary Applicators

Two kinds of endocavitary applicators have been developed:

1) The first one (Fig. 2) designed for urethra, is made with a plastic flexible double catheter (Foley type urological catheter), which outer diameter is equal to 6 mm. A flexible coaxial cable (external diameter $\emptyset$ = 2.2 mm), at the end of which the outer conductor is removed on a length h is inserted in the inner catheter. In order to avoid hot spots at the applicator urethra interface, a water cooling circulation is made in the catheter. The total

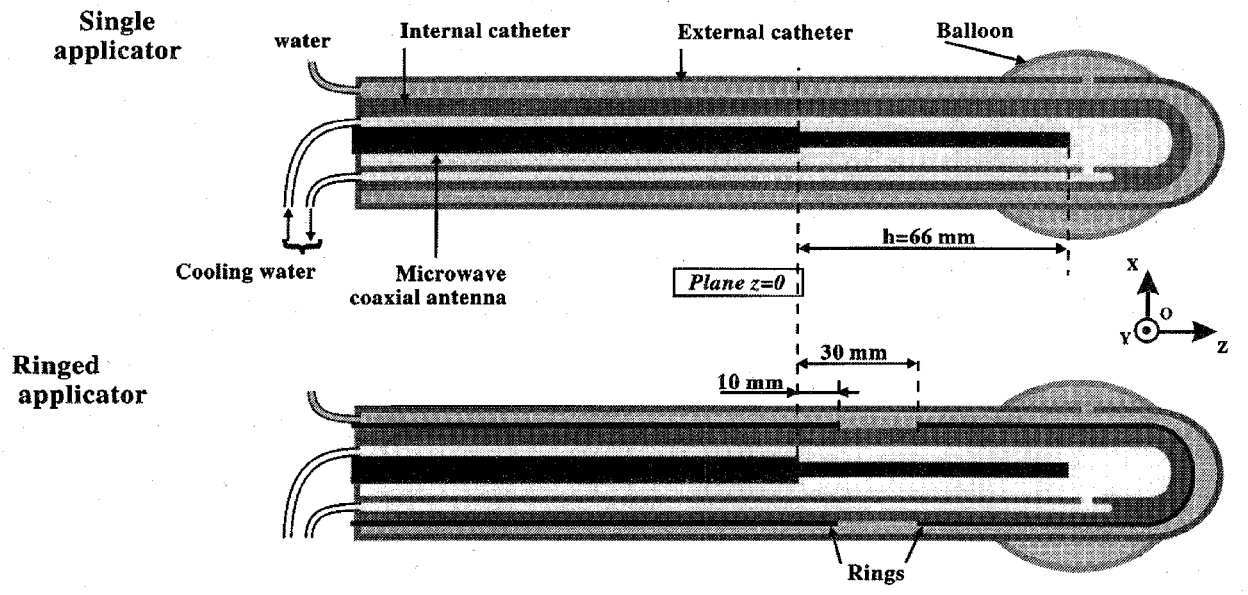

Fig. 2. Description of the two kinds of urethral microwave applicators: single and ringed models.

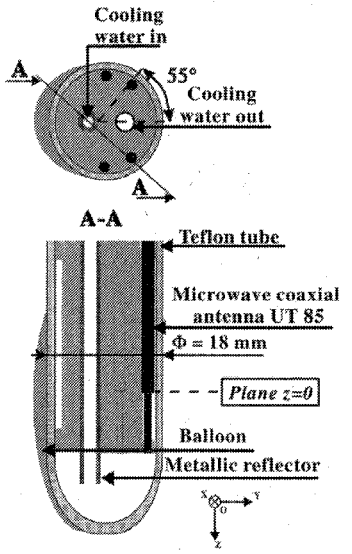

Fig. 3. Description of a rectal microwave applicator with 4 coaxial antennas.

length of the applicator is about 50 cm. The external catheter is ended with an inflatable balloon to allow an accurate positioning of the applicator in the urethra in order to be situated on the level of the prostate gland for the treatment. Because the frequency bandwidth around 915 MHz is now reserved for cellular phones in Europe, another authorized frequency, that is to say 434 MHz is used. For this frequency, the radiating diagram spreads on a too long distance for the treatment of the prostatic adenoma and is likely to cause damages to the sphincter or to the bladder cervix. So, it is necessary to design another urethral applicator: the second generation uses metallic rings on the external wall of the inner catheter which allows to erase some parts of the radiating diagram [Fig. 2(b)].

TABLE I

	along OX	along OY	along OZ
dimension (mm)	20	20	150
step (mm)	0.2	0.2	0.5
number of points	101	101	301

2) The second one is a rectal applicator which includes several antennas (two, four, or more) made from semi-rigid coaxial cable (UT85 standard) (external diameter $\emptyset$ = 2.2 mm) associated with a cylindrical metallic reflector to focus the microwave energy in the prostate gland (Fig. 3). Both antenna and reflector are slid in a teflon tube which includes a cooling system by water flowing in order to avoid burns of the rectum wall.

III. Description of the Numerical Method

A. The FDTD Method

In order to take into account the heterogeneousness of the volume surrounding the antenna, but also the exact shape of tissues and applicators, a complete three–dimensional (3-D) model based on the FDTD method has been developed.

The FDTD method was first proposed by Yee [2] and later developed, extended, and simplified by several authors [3]–[6]. This well-known method, is widely used for solving electromagnetic problems [7], [8] and has also been recognized as a useful tool for calculating the interactions of electromagnetic waves with human tissues, particularly for medical applications such as hyperthermia [9]–[12]. The electromagnetic problem consists of numerically solving the Maxwell's

TABLE II
(H, H') VALUES GIVING A GOOD MATCHING (THE REFLECTION COEFFICIENT S_{11} IS ALWAYS SMALLER THAN −15 dB)

Frequency	915 MHz				434 MHz						
h (mm)	14	20	25	30	50	40	35	30	25	20	15
h' (mm)	7	5	3	0.5	1	5	7	8	11	13	17

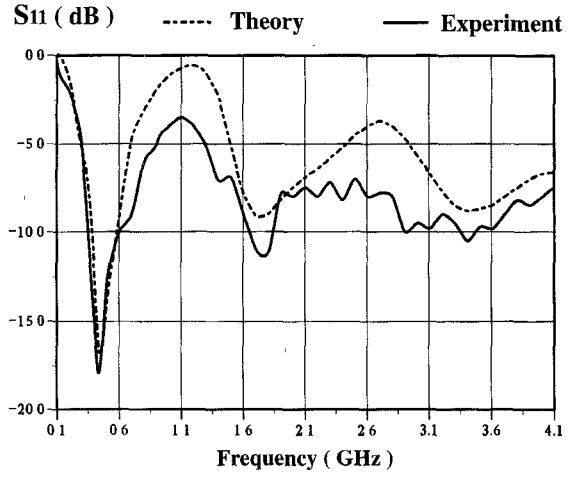

Fig. 4. Experimental (full line) and theoretical (dotted line) variations of the reflection coefficient (S_{11} parameter) as a function of frequency for the interstitial applicator (with h = 40 mm and h' = 5 mm).

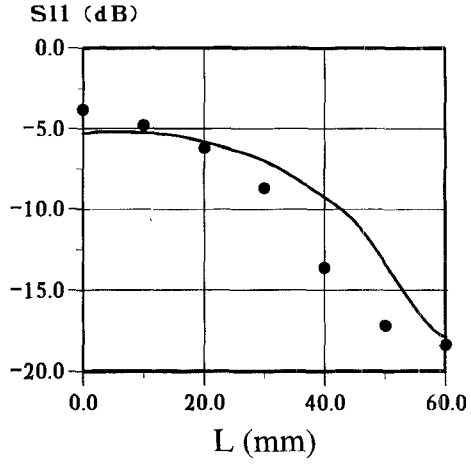

Fig. 5. Theoretical (full line) and experimental (dots) variations of the reflection coefficient (S_{11} parameter) as a function of the length L, distance between the end of the antenna and the interface tissues-air.

curl equations in which finite-difference approximations are employed for both time and space derivatives. The FDTD technique proceeds by segmenting the structure and the surrounding space into a 3-D mesh composed of a number of rectangular unit cells. The E and H fields positioned at half-step intervals around the unit cell, are evaluated at alternative half time steps, effectively giving centered difference expressions for both the space and time derivatives. To ensure stability, the time step Δt must satisfy the following stability criterion [3] $\Delta t \leq 1/\left[v_{\max}\sqrt{(1/\Delta x^2)+(1/\Delta y^2)+(1/\Delta z^2)}\right]$ where Δx, Δy, and Δz are the space steps corresponding to the dimensions of the elementary FDTD unit cell. For example, the incremental space values along the three axes used for the FDTD calculation of the ringed urethral applicator are given in Table I. It is possible to take into account the symmetries of the structure to reduce the CPU time.

Another basic problem with any finite difference solution of Maxwell's equations is the treatment of the field components at the lattice truncation. Because of the limited computer storage, the lattice must be restricted in size. Proper truncation of the lattice requires that any outgoing wave disappear at the lattice boundary without reflection during the continuous time stepping of the algorithm. An absorption boundary condition for each field component is therefore needed at the edge of the lattice. In this paper, Mur's first-order approximate absorbing boundary conditions are used [13]. Second-order absorbing boundary conditions have been also tested, but the results show that the first-order absorbing boundary treatment is sufficiently accurate. It should be noted that for the calculations in lossy regions, such as those presented in this paper, the absorbing boundary conditions are not as critical as for the free-space scattering problems.

With this program, we obtain the following theoretical results:

1) Variations of the reflection coefficient (S_{11} parameter) as a function of frequency. We have the possibility (not used in the results presented) to take into account the frequency dependence of dielectric properties of media [(FD)^{2}TD model] [12].
2) Power deposition inside the heated lossy media. Once the electric field is found, the specific absorption rate distribution (SAR) can be computed. The normalized SAR (we assume the density ρ to be equal to 1 everywhere) is defined using the following formula as:

$$\mathrm{SAR}(i,j,k) = \frac{\sigma}{2}\left[|E_x(i,j,k)|^2_{\max}+|E_y(i,j,k)|^2_{\max}+|E_z(i,j,k)|^2_{\max}\right]$$

where $E_{x_{\max}}$, $E_{y_{\max}}$, and $E_{z_{\max}}$ are the maximum steady-state electric field components at cell (i, j, k).
3) Heating patterns obtained from the 3-D resolution of the bioheat transfer equation using the previous electromagnetic computation of the absorbed power by tissues. It is possible to obtain transversal and longitudinal thermal patterns.

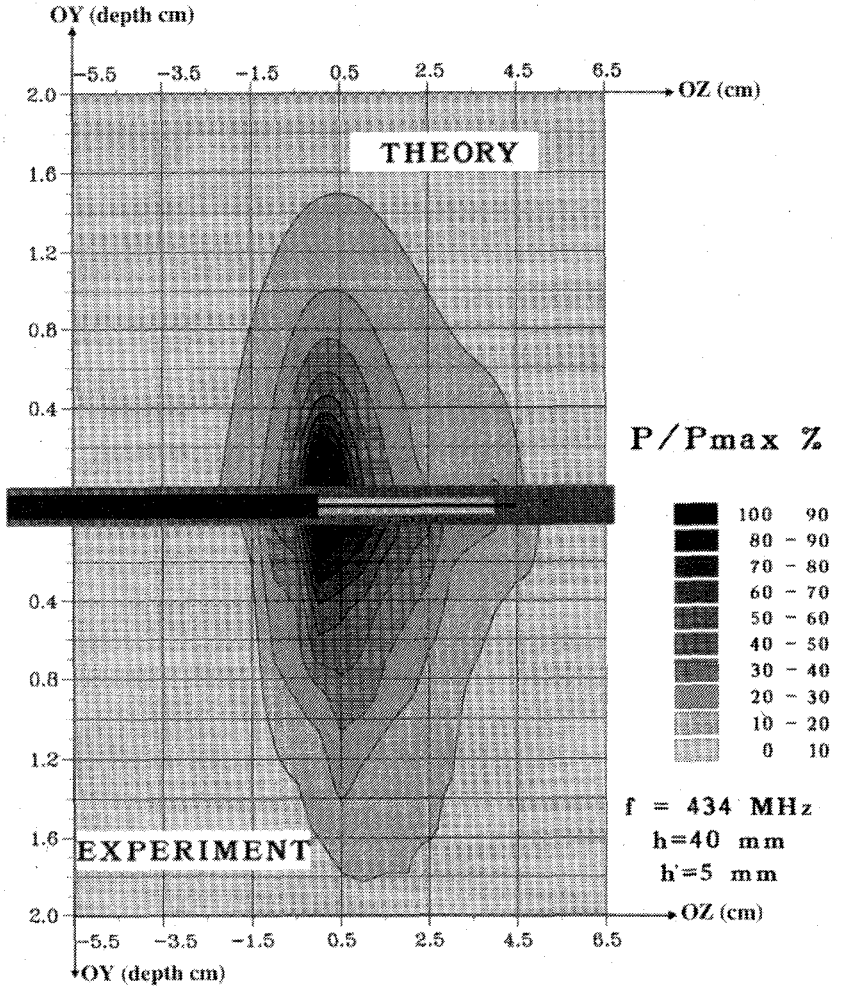

Fig. 6. Comparison between measured and calculated longitudinal power deposition diagram obtained at 434 MHz for the interstitial applicator entirely dipped in salt water at 6 g/l (with h = 40 mm and h' = 5 mm).

B. Calculation of the Temperature Distribution

The spatial distribution of temperature in lossy medium during the plateau phase of hyperthermia session is described by the bioheat transfer equation in the steady-state

$$k_t(x, y, z).\left[\frac{\partial^2 T(x, y, z)}{\partial x^2}+\frac{\partial^2 T(x, y, z)}{\partial y^2}+\frac{\partial^2 T(x, y, z)}{\partial z^2}\right] + B(x, y, z)+P_a(x, y, z)=0$$

where x, y, z are space variables, $k_t(x, y, z)$ tissues thermal conductivity, $P_a(x, y, z)$ the absorbed microwave power density inside tissues (obtained from the FDTD method) and $T(x, y, z)$ the temperature. The convective heat transfer $B(x, y, z)$ between tissues and arterial blood (at temperature T_a) takes the following form: $B(x, y, z) = v_s(x, y, z)\,.\,[T_a - T(x, y, z)]$ with $v_s(x, y, z)$ the blood flow parameter inside tissues (this value is different according to tissue types).

The bioheat transfer equation is solved according to the method of discrete finite differences. We obtain a system of differential equations which is solved using an iterative method based on the "Cholesky method" [14], [15] in which some coefficients have been introduced in order to increase the convergence speed of the solution. The heterogeneous character of the medium can be taken into account, particularly the blood flow term v_s different in each type of tissue (skin, fat, muscle, tumor, ...) and also the thermal conductivity k_t. For example, for the polyacrylamide gel we have: k_t = 0.38 W.m^{-1}.°C^{-1}; v_s = 1500 W.m^{-3}.°C^{-1}; T_a is close to 20°C (temperature of the room).

IV. Experimental Measurements

In order to determine the potential performances of these applicators, experimental measurements were also carried out on phantom models of human tissues (saline solution at 6 g/l or polyacrylamide gel).

First, the return loss (S_{11} parameter) has been measured as a function of frequency by means of a network analyzer HP 8510 in order to obtain the resonant frequency of the applicator and the level of adaptation of the applicator at the heating frequency [transfer of at least 90% the microwave energy to the volume to be heated not only at the heating frequency but also in a wide bandwidth around the central frequency (3 GHz) of the radiometer used for temperature measurement and monitoring: that corresponds to a S_{11} parameter less than -10 dB].

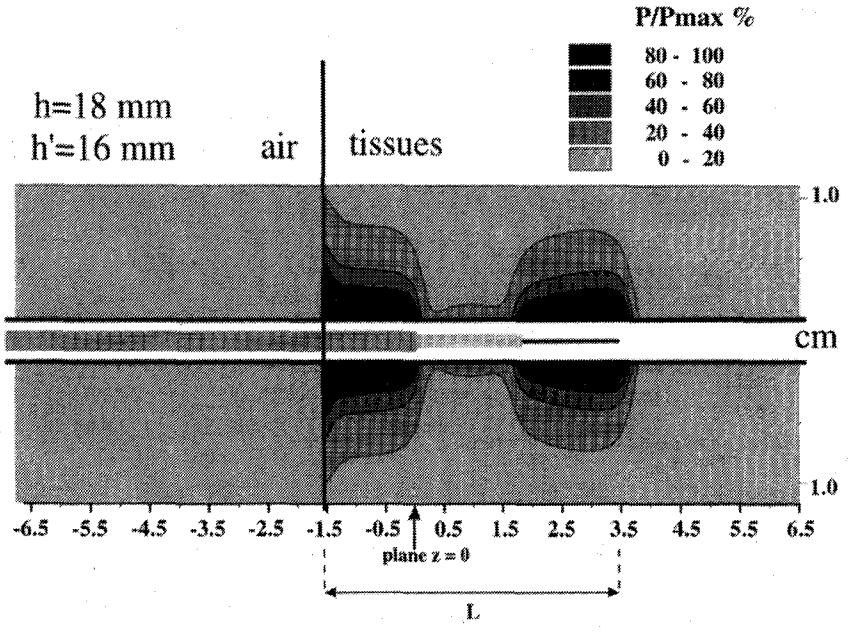

Fig. 7. Calculated longitudinal power deposition diagram obtained at 434 MHz for the interstitial applicator (h = 18 mm and h' = 16 mm) dipped in salt water at 6 g/l for a distance L equal to 50 mm.

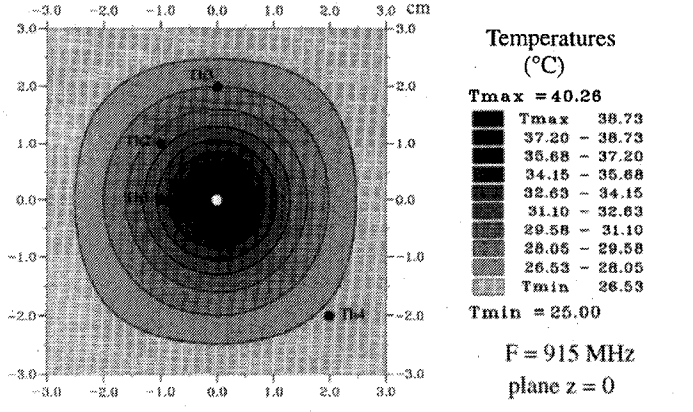

Temperatures (°C)

	Experiment	Theory
Th1	33.0	32.5
Th2	31.0	30.4
Th3	28.3	28.2
Th4	26.2	26.3

Fig. 8. Comparison between calculated heating pattern in the plane z = 0 for the coaxial antenna (h = 40 mm and h' = 5 mm) at 915 MHz and measured temperatures obtained by thermocouples inserted in the polyacrylamide gel.

The second step of the experiment consists in the determination of the energy distribution of the applicator radiating into a lossy medium coupled with it. Two methods can be used.

1) In the first one, we determine the electric field pattern created in a saline solution at 6 g/l (equivalent to human tissues) by the microwave applicator under test [16], [17] with a simple system for mapping the electric field. An electric probe, which can be moved in the three directions within the solution, is connected to a voltmeter via a square-law diode detector. We used a 2 mm long dipole, the direction of which was parallel to the antenna. The accuracy of the probe position is about 0.5 mm. The detected voltage is proportional to the squared electric field intensity (E^2) and consequently to the dissipated power within the lossy medium. The SAR error is depending on the dipole used and on its orientation.
2) The second method is based on the measurement of the temperature increase in a polyacrylamide gel, induced by microwave power for a short time (about one minute) in

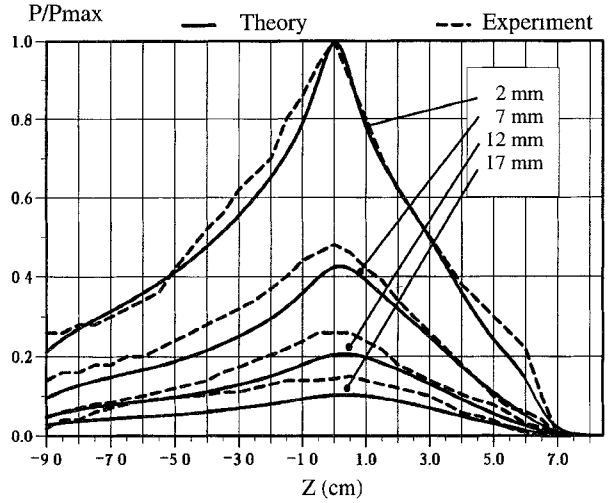

Fig. 9. Comparison between calculated (full line) and measured (dotted line) longitudinal power deposition diagrams obtained at 434 MHz for the two kinds of urethral applicators dipped in salt water at 6 g/l. (a) Related to the single applicator. (b) Related to the ringed applicator.

order to avoid the thermal conduction phenomena inside the gel. The increase of temperature is then proportional to the dissipated power inside the gel.

These two different techniques give us the SAR pattern and the microwave penetration depth δ in the lossy medium at the different heating frequencies (434 and 915 MHz in this study).

We have also characterized the thermal performances of the applicators. This is obtained from the temperature measurement performed on a polyacrylamide gel after a heating session of about 45 minutes using an automatic experimental system [12]. In this polyacrylamide gel, catheters are inserted parallel and regularly spaced 1 cm apart in a vertical plane. The array of thermocouple probes is moved by a stepper motor inside and outside of these catheters. The data system measurement controls the motions of this stepper motor and records the temperatures of the probes. It is to be noted that the temperature measurements are taken when the generator is switched off.

V. Results and Discussion

A. Interstitial Applicators

A systematic study of the lengths h and h' was then carried out at 434 and 915 MHz (Table II): it appears that for a chosen length h, only one value of h' corresponds which gives the best matching. As an example, we give on Fig. 4 the variations of the reflection coefficient as a function of frequency for a coaxial antenna made with h = 40 mm and h' = 5 mm and entirely dipped in a saline solution at 6 g/l: we can note a good agreement between theoretical results obtained by the FDTD method and experimental measurements. In the case of the treatment of breast cancer, the interstitial antenna is driven in tissues. In order to obtain a good radiating diagram, it is necessary to study the level of adaptation of this antenna as a function of the driving in distance inside the tissues which has been called L (see Fig. 1): L is the distance between the end of the antenna and the interface tissues-air. The results concerning the evolution of the reflection parameter S_{11} as a function of the distance L are given on the Fig. 5: in this case, the antenna is partially dipped in a saline solution at 6 g/l. We can note that the distance L must be greater than 40 mm in order to obtain a good level of adaptation ($S_{11} < -10$ dB).

In the Fig. 6, we present the theoretical and experimental results related to the power radiated pattern at 434 MHz for the same coaxial antenna (h = 40 mm and h' = 5 mm) entirely dipped in a saline solution at 6 g/l. The absorbed power deposition has been normalized to the maximum value in the volume. A good agreement between theory and experiment can be noted. We have also studied the radiating diagram when the antenna is partially dipped in tissues. We have calculated the SAR in a longitudinal plane for a structure constituted with air and saline solution at 6 g/l when the antenna is driven in for a distance L equal to 50 mm for which the level of adaptation is good (the S_{11} parameter is equal to -17 dB). The results are presented in the Fig. 7. We observe that the shape of this radiating diagram is quite different from the one obtained previously when the antenna is entirely dipped in salt water. It is to be noted that the deposited power has been calculated using the following formula $P = [(\sigma/2)(|E|^2)]$: we have no power in the media constituted with air because σ = 0. So, it will be necessary to have a distance L greater than $2(h + h')$ in order to obtain a power deposition diagram with a maximum value in the plane $z = 0$.

The comparison between the theoretical thermal pattern obtained for 915 MHz and the experimental measurements obtained with thermocouples inserted in the polyacrylamide gel is presented on the Fig. 8. Assuming the real part R_e of the entrance impedance of the antenna to be equal to 50 Ω at the heating frequency, we determine the power P by the formula $P = \frac{1}{2}(V_M^2/R_e)$ with $V(t) = V_M \cos(\omega t)$, theoretical voltage at the entrance of the antenna. As the medium is a linear one, it is easy to obtain the experimental value of P by varying the value of V_M. We can note that the agreement between theory and experiment is quite good.

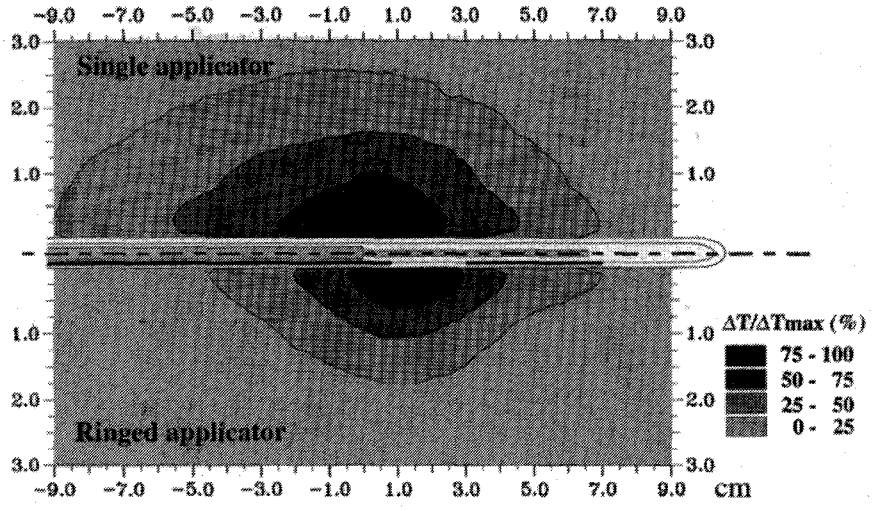

Fig. 10. Comparison between experimental longitudinal heating patterns obtained at 434 MHz for the two kinds of urethral applicators (the lossy medium is polyacrylamide gel).

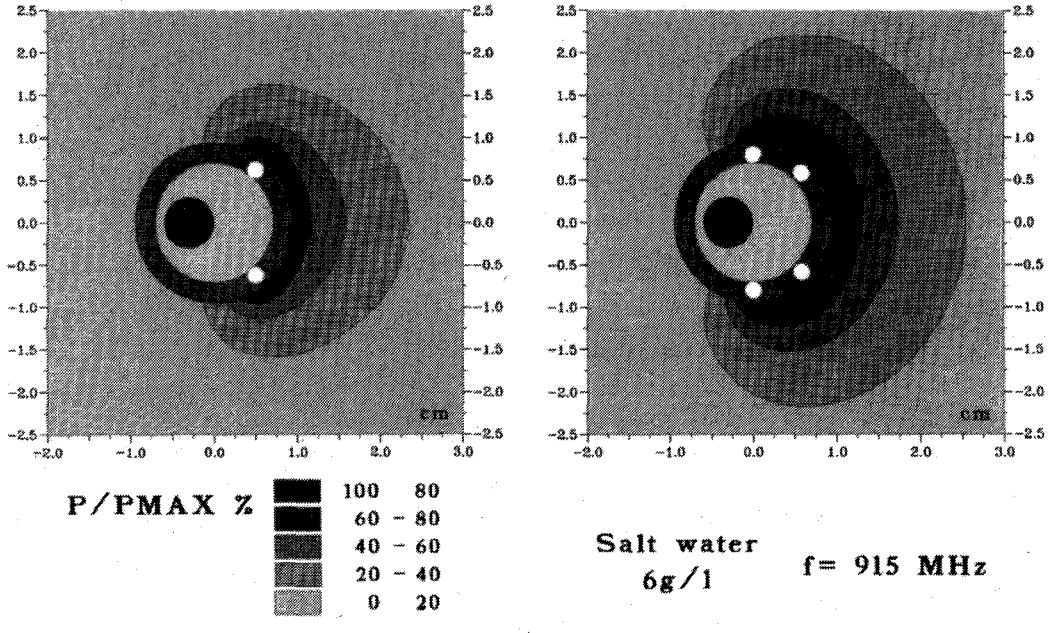

Fig. 11. Comparison between calculated power deposition diagram obtained in the plane $z = 0$ for the rectal applicators with 2 and 4 antennas (the lossy medium is salt water at 6 g/l and the heating frequency 915 MHz).

B. Endocavitary Applicators

With regard to the urethral applicator, the results concerning the reflection coefficient are similar to the ones of the interstitial antenna.

In order to verify the influence of the rings introduced on the urethral applicator in order to reduce the radiating diagram, we have calculated the isopower longitudinal curves at 434 MHz for the two previously described applicators (Fig. 9). These results show that the radiating diagram of the ringed applicator extends less than the first applicator. In fact, the 40% isopower curve spreads on 90 mm for the single applicator and only on 60 mm for the ringed one: this confirms the interest of the rings. In order to verify these results, we have calculated the thermal patterns of the two applicators. The comparison is given in the Fig. 10 and shows clearly the reduction of the heated zone for the ringed applicator.

For the rectal applicator, we have determined the power deposition in a saline solution (at 6 g/l) at 915 MHz in the plane $z = 0$ cm (where the deposited power is maximum [18], [19]). The 2D theoretical results for the rectal applicators with 2 and 4 coaxial antennas are given on Fig. 11: we can observe the effect of the metallic reflector which focus the energy in one direction in contrast with the diagram of one antenna which is symmetrical. Experimental measurements confirms

these results. More the applicator with four antennas spreads on a longer distance and covers a greater area.

VI. Conclusion

We have developed a complete 3-D model based on the FDTD method for the study of interstitial and intracavitary applicators. With this model, we have modeled several kinds of applicators with a heterogeneous lossy media. This study yields a complete choice of applicators different in their geometric parameters, able to heat tumors of various sizes. The theoretical results obtained with the FDTD method have been compared to experimental measurements and show a good agreement.

The perspectives of this work are the following:

1) For the interstitial applicator, a phased array of antennas (until 12) allowing to treat tumors situated in locations with difficult access (basis of tongue) is still working in a microwave hyperthermia system.
2) For the endocavitary applicators, rather than use separately the urethral or the rectal applicator for the benign prostatic hyperplasia treatment, a solution consists in using simultaneously both applicators as to realize the technique we have called "crossed fire."

These directions of research works are still ongoing and the first results will be soon published.

References

[1] M. Chivé, "Use of microwave radiometry for hyperthermia monitoring and as a basis for thermal dosimetry," in *Methods of Hyperthermia Control, Series on Clinical Thermology, Subseries Thermotherapy,* M. Gautherie, Ed Heidelberg: Springer-Verlag, 1990, vol. 3, pp. 113–128.

[2] K. S. Yee, "Numerical solution of initial boundary value problems involving Maxwell's equations in isotropic media," *IEEE Trans. Antennas Propagat.,* vol. AP-14, no. 3, pp. 302–307, May 1966.

[3] A. Taflove and M. E. Brodwin, "Numerical solution of steady-state electromagnetic scattering problems using the time-dependent Maxwell's equations," *IEEE Trans. Microwave Theory Tech.,* vol. MTT-23, no. 8, pp. 623–630, Aug. 1975.

[4] ——, "Computation of the electromagnetic fields and induced temperatures within a model of the microwave-irradiated human eye," *IEEE Trans. Microwave Theory Tech.,* vol. MTT-23, no. 11, pp. 888–896, Nov. 1975.

[5] R. Holland, L. Simpson, and K. S. Kunz, "Finite-difference analysis of EMP coupling to lossy dielectric structures," *IEEE Trans. Electromag Compat.,* vol. EMC-22, no. 3, pp. 203–209, Aug. 1980

[6] K. Umashankar and A. Taflove, "A novel method to analyze electromagnetic scattering of complex objects," *IEEE Trans Electromag. Compat.,* vol. EMC-24, no. 4, pp. 397–405, Nov. 1982.

[7] X. Zhang and K. K. Mei, "Time-domain finite-difference approach to the calculation of the frequency-dependent characteristics of microstrip discontinuities," *IEEE Trans. Microwave Theory Tech.,* vol. 36, no. 12, pp. 1775–1787, Dec. 1988.

[8] D M. Sheen, S M. Ali, M. D. Abouzahra, and J. A. Kong, "Application of the three-dimensional finite-difference time-domain method to the analysis of planar microstrip circuits," *IEEE Trans. Microwave Theory Tech.,* vol. 38, no. 7, pp 849–857, July 1990.

[9] D. M. Sullivan, D. T. Borup, and O. M. P. Gandhi, "Use of the finite-difference time-domain method in calculating EM absorption in human tissues," *IEEE Trans. Biomed. Eng.,* vol. BME-34, no 2, pp. 148–157, Feb. 1987.

[10] D. M. Sullivan, O. M. P. Gandhi, and A Taflove, "Use of the finite-difference time-domain method for calculating EM absorption in man models," *IEEE Trans. Biomed. Eng.,* vol. BME-35, no. 3, pp. 179–186, Mar. 1988.

[11] D. M. Sullivan, "Three-dimensional computer simulation in deep regional hyperthermia using the FDTD method," *IEEE Trans. Microwave Theory Tech ,* vol. 38, no 2, pp. 204–211, Feb. 1990.

[12] P.-Y. Cresson, C Michel, L. Dubois, M. Chivé, and J. Pribetich, "Complete three-dimensional modeling of new microstrip-microslot applicators for microwave hyperthermia using the FDTD method," *IEEE Trans. Microwaves Theory Tech.,* vol. MTT-42, no. 12, pp. 2657–2666, Dec 1994.

[13] G. Mur, "Absorbing boundary conditions for finite difference approximation of the time domain electromagnetic field equations," *IEEE Trans. Electromag. Compat.,* vol. EMC-23, no. 4, pp. 377–382, Nov 1981.

[14] J. P. Nougier, "Méthodes de calcul numérique," Masson, Ed., 1983.

[15] A. Ralston and H. S. Wilf, "Méthodes mathématiques pour calculateurs arithmétiques," Dunod, Ed , 1965.

[16] J -C. Camart, J.-J. Fabre, B. Prévost, J. Pribetich, and M. Chivé, "Coaxial antenna array for 915 MHz interstitial hyperthermia Design and modelization—Power deposition and heating pattern—Phased array," *IEEE Trans. Microwaves Theory Tech.,* vol. 40, no. 12, pp 2243–2250, Dec. 1992.

[17] G. Gajda, M. A. Stuchly, and S. S. Stuchly, "Mapping of the near-field pattern in simulated biological tissues," *Electron Lett ,* vol 15, no. 4, pp. 120–121, Feb. 15, 1979.

[18] R. W. P. King, B. S. Trembly, and J. W. Strohbehn, "The electromagnetic field of an insulated antenna in a conducting or dielectric medium," *IEEE Trans. Microwave Theory Tech.,* vol. MTT-31, no. 7, pp. 574–583, July 1983.

[19] J. P. Casey and R. Bansal, "The near field of an insulated dipole in a dissipative dielectric medium," *IEEE Trans. Microwave Theory Tech.,* vol. MTT-34, no. 4, pp 459–463, Apr. 1986

Jean-Christophe Camart, for a photograph and biography, see this issue, p. 1761.

David Despretz, for a photograph and biography, see this issue, p. 1767.

Maurice Chivé, for a biography, see this issue, p. 1761.

Joseph Pribetich, for a photograph and biography, see this issue, p. 1761.